Aalto University

OPEN ACCESS

This is an electronic reprint of the original article.
This reprint may differ from the original in pagination and typographic detail.

Lehtomäki, Matti; Kukko, Antero; Matikainen, Leena; Hyyppä, Juha; Kaartinen, Harri; Jaakkola, Anttoni

Power line mapping technique using all-terrain mobile laser scanning

Published in:
Automation in Construction

DOI:
10.1016/j.autcon.2019.03.023

Published: 01/09/2019

Document Version
Publisher's PDF, also known as Version of record

Published under the following license:
CC BY-NC-ND

Please cite the original version:
Lehtomäki, M., Kukko, A., Matikainen, L., Hyyppä, J., Kaartinen, H., & Jaakkola, A. (2019). Power line mapping technique using all-terrain mobile laser scanning. *Automation in Construction*, *105*, Article 102802. https://doi.org/10.1016/j.autcon.2019.03.023

This material is protected by copyright and other intellectual property rights, and duplication or sale of all or part of any of the repository collections is not permitted, except that material may be duplicated by you for your research use or educational purposes in electronic or print form. You must obtain permission for any other use. Electronic or print copies may not be offered, whether for sale or otherwise to anyone who is not an authorised user.

Automation in Construction 105 (2019) 102802

Contents lists available at ScienceDirect

Automation in Construction

journal homepage: www.elsevier.com/locate/autcon

Power line mapping technique using all-terrain mobile laser scanning

Matti Lehtomäki[a,*], Antero Kukko[a,b], Leena Matikainen[a], Juha Hyyppä[a], Harri Kaartinen[a,c], Anttoni Jaakkola[a]

[a] Finnish Geospatial Research Institute FGI, Department of Remote Sensing and Photogrammetry, Geodeetinrinne 2, 02430 Masala, Kirkkonummi, Finland
[b] Aalto University School of Engineering, Department of Built Environment, Otakaari 4, P.O. Box 15800, 00076 Aalto, Espoo, Finland
[c] University of Turku, Department of Geography and Geology, Vesilinnantie 5, FI-20014 Turku, Finland

ARTICLE INFO

Keywords:
Mobile laser scanning
Lidar
Power line corridor
Inspection
Feature extraction
All-terrain
Forest

ABSTRACT

Power line mapping using remote sensing can automate the traditionally labor-intensive power line corridor inspection. Land-based mobile laser scanning (MLS) can be a good choice for the power line mapping if an aerial inspection is impossible, too costly or slow, unsafe, prohibited by regulations, or if more detailed information on the power line corridor is needed. The mapping of the power lines using MLS was studied in a rural environment outside the road network for the first time. An automatic power line extraction algorithm was developed. The algorithm first found power line candidate points based on the shape and orientation of the local neighborhood of a point using principal component analysis. Power lines were retrieved from the candidates using random sample consensus (Ransac) and a new power line labeling method, which takes into account the three-dimensional shape of the power lines. The new labeling method was able to find the power lines and remove false detections, which were found, for example, from the forest. The algorithm was tested in forested and open field (arable land) areas, outside the road environment using two different platforms of MLS, namely, personal backpack and all-terrain vehicle. The recall and precision of the power line extraction were 93.3% and 93.6%, respectively, using 10 cm as a distance criterion for a successful detection. Drifting of the positioning solution of the scanner was the largest error source, being the (contributory) cause for 60–70% of the errors. The platform did not have a significant effect on the power line extraction accuracy. The accuracy was higher in the open field compared to the forest, because the one-dimensional point density along the power line was inhomogeneous and GNSS (global navigation satellite system) signal was weak in the forest. The results suggest that the power lines can be mapped accurately enough for inspection purposes using MLS in a rural environment outside the road network.

1. Introduction

Uninterrupted delivery of electricity is a prerequisite for an efficient functioning of a modern society. In rural environments, outside the road network (e.g., forest) many threats exist in the corridors of overhead power lines, which may disturb the transmission and distribution of electric power. Short circuits, blackouts, and forest fires are examples of problems, which trees and other high vegetation near the power lines give rise to [3,32,40,43]. Falling trees damage the power line components especially in stormy conditions, which may result in power outages. Crown snow-load bends the trees causing a risk of contact with the power line, and consequently disturbance in the power delivery. Also, deterioration of power line components, such as corrosion, insulators cracks, and mechanical damage in the conductors is a problem encountered in all environments [1,54]. The deterioration can follow from a movement caused by wind, a poor manufacturing quality, or a poor installation quality [1,54]. In some areas, storms, landslides and floods can cause serious damage to the power lines [2,52]. Therefore, it is important to inspect the condition of the power line corridor at regular intervals. Traditional inspection techniques, in which the corridors are visually inspected either by foot or from a helicopter, are labor intensive and subject to a human error [3,40].

Remote sensing is a promising technique for the efficient and objective inspection of the power lines. Remotely sensed data sources range from satellite images to detailed photographs taken on the ground or by climbing robots, and a large number of remote sensing methods have been presented for power line monitoring in research literature [40]. In principle, remote sensing fixes the problems of the

* Corresponding author.
E-mail addresses: matti.lehtomaki@nls.fi (M. Lehtomäki), antero.kukko@nls.fi (A. Kukko), leena.matikainen@nls.fi (L. Matikainen), juha.coelasr@gmail.com (J. Hyyppä), harri.kaartinen@nls.fi (H. Kaartinen), anttoni.jaakkola@gmail.com (A. Jaakkola).

https://doi.org/10.1016/j.autcon.2019.03.023
Received 20 November 2018; Received in revised form 6 February 2019; Accepted 28 March 2019
0926-5805/ © 2019 The Authors. Published by Elsevier B.V. This is an open access article under the CC BY-NC-ND license (http://creativecommons.org/licenses/BY-NC-ND/4.0/).

traditional monitoring approaches. First, it is an efficient technique, as large areas can be covered with low efforts. Second, if the remotely sensed data can be interpreted using automatic computer vision algorithms, the assessment is no longer dependent on a subjective human visual interpretation. Additionally, the data on the power lines will be available for later reanalyzes.

Mobile laser scanning (MLS) with dense point clouds is an active remote sensing technique that has gained a lot of interest in the recent years [33,45,46]. It is well suited for corridor mapping, and it complements the more traditional airborne laser scanning (ALS) and also a more novel unmanned aerial vehicle (UAV) based laser scanning techniques. MLS provides more detailed information on the power line corridor than aerial sensors and from a different viewing point, because it operates on the ground level and closer to the power line. For example, power lines, narrow wooden poles, and vegetation below the forest canopy can be mapped in more detail (Fig. 3), which can be utilized in more advanced monitoring and maintenance operations. An MLS system and its operation are cheaper compared to heliborne ALS, and MLS could be used as a cost-efficient method to fill gaps remaining after an aerial campaign. Gaps may exist, for example, due to flying restricted areas or along complex networks. Because the flying costs are high, one possible cost-efficient combination could be to fly faster, for example, using a fixed-wing aircraft, which is much cheaper than using a helicopter, and thus save in the data acquisition costs. Faster flying speed inevitably causes more gaps, for example, in the curves and in areas of complex networks. The gaps can be filled using MLS, whose mobilization costs are lower than those of ALS. In other words, it might be cheaper to fill the gaps using MLS instead of flying so slow that hardly any gaps remain. MLS could also be used—possibly together with UAV—when there is a need to have higher-quality information from interest areas detected with ALS. MLS can be operated in more challenging weather conditions than the flying systems, and, for example, moderate wind does not cause problems. MLS can also be combined with a UAV to gain better coverage of the power line and other components from different viewing points [39]. Overall, MLS can be considered as a complementary data to airborne surveys.

So far, MLS has been applied in the mapping of the power lines in an urban environment [12,17,29,56] and in a road environment [56]. MLS-based mapping of power lines in the urban environment is well justified, because flying with a UAV or helicopter is difficult and inefficient there. The above-mentioned gaps in the data occur in all areas, thus also outside the road network and in heavy forests. However, no reports on the application of MLS outside the road network including forest have been published so far. When considering the power line corridor mapping, areas outside the road network differ from urban and road environments, for example, in the ground surface roughness, mobility restrictions (e.g., vegetation, rough terrain, rocks), and GNSS (global navigation satellite system) satellite visibility (trees blocking the signals). Because of these, the positioning accuracy of the MLS system is worse and the point density in the direction of the trajectory in the point clouds is more heterogeneous outside the road environment. Therefore, the automatic extraction of power line components is more challenging outside the road network compared to an urban or road environment. However, it should be noted that in the urban areas high buildings also block the GNSS signal. In corridor mapping business in Europe and USA, data acquisition costs dominate in the total costs, and thus new acquisition techniques could have a remarkable business potential.

In this paper, the automatic mapping of the power lines is studied in a rural environment, outside the road environment; that is, in the forest and arable land. The main contribution of this article is two-fold. First, the feasibility of the MLS technology in the power line mapping is demonstrated outside the road environment for the first time, both in forested and non-forested areas. Second, a novel algorithm is developed that extracts power lines from MLS point clouds automatically. The novelty of the algorithm is justified in Section 2.2. We also demonstrate that most of the power line poles can be extracted with an automatic method that uses rather simple principles and algorithms from previous MLS studies. The accuracy of the developed methods is evaluated experimentally using data collected both with a personal backpack laser scanner and a scanner mounted on an all-terrain vehicle (ATV). Neither of the platforms has been applied in the MLS-based power line mapping previously. In this paper, we compare the performance of the developed algorithm in the open field to that in the forested area. A comparison is also performed between the backpack data and the ATV data.

2. Background

2.1. The laser scanning methods in the mapping of power line corridors

Airborne laser scanning (ALS) is an important remote sensing technique that has gained popularity in both research and practical monitoring work during the last two decades. ALS is an active technique based on the lidar (light detection and ranging) principle, and it produces accurate three-dimensional (3D) point clouds with *x*-, *y*-, and *z*-coordinates and a return intensity [7]. The ALS data over power lines is normally acquired from a helicopter, and the point density is typically tens of points per m^2 but can be even hundreds of points per m^2. A typical absolute accuracy of the points is roughly 5–10 cm in the horizontal plane and 2–5 cm in the vertical direction on hard surfaces [40]. Such data can be utilized to map the shape of power lines accurately. Detailed modeling of power lines with catenary curves has been discussed, for example, in [41]. Recently, laser scanning from UAVs has also become possible [5,24,25]. This is likely to become a popular technique in the future as it gives more flexibility for the data acquisition and reduces the costs. ALS, either from helicopters or UAVs, sees power lines and their surroundings from above, which is advantageous for the mapping of the power lines and trees near to them. However, it also means that vertical poles and small components are not necessarily clearly visible in the data. Tree cover can also limit the visibility of power lines, and weather conditions can restrict the ability to fly over the power lines.

Compared to ALS, MLS is a newer technology, which has been applied so far mostly in the precise mapping of urban and street environments. It is especially suitable for corridor type of applications (e.g., roads) and power lines are to a certain extent well-defined corridor type objects of interest. MLS provides with ease of deployment and data collection with good precision and level of detail for asset modeling and monitoring. The mapping is not limited to the power line itself, but it can generate accurate information on the terrain and vegetation in the close proximity of the line (Fig. 3). Outside the roads, the mobility within the corridor can be achieved by using an all-terrain vehicle (ATV), or deploying a specific backpack mounted lidar system for the mapping task, also called personal laser scanning (PLS) [22].

The main advantages of MLS over ALS surveys are higher detail from close to the objects of interest and operability in more challenging weather conditions (e.g., wind). Acquisition cost of an MLS system is cheaper, and there are multiple lidar sensors in the market to choose from to meet the needs of the grid operator. Also operation cost is considerably lower than that of, for example, heliborne ALS. However, MLS cannot provide wide area data, especially when the terrain conditions are inoperable for an ATV or other wheeled platforms. Lower acquisition and maintenance costs permit multiple systems for the price of an ALS system, so more time-space efficient fleet could be used for better mileage.

MLS operates at the ground level and thus substantially closer to the power lines than ALS (0–20 m distance to the power line in MLS; typically at least tens of meters in ALS). Therefore, both the point density of MLS (even > 1000 points per m^2 at a 10-m range from the scanner) and 3D precision of MLS (2–3 cm in good GNSS conditions, see [19,27,34]) are considerably higher than those of the ALS data. Higher point density enables the mapping of the surrounding environment

more thoroughly and higher 3D accuracy of the point cloud makes it possible to retrieve more accurate features, such as surface normals and pole or trunk diameters. Also, the beam size of the laser (i.e., footprint) is small in MLS compared to ALS, which enables the mapping of pylons and assets in detail. Therefore, MLS maps the power line components and the power line corridor in more detail than ALS. Compared to ALS, the scanning geometry of MLS is better suited for the mapping the power line components [40]. Power lines on top of each other are difficult to detect from the ALS data due to vertical scanning pattern as the uppermost power line shadows the ones below it from the top view. Instead, such power lines are typically well visible in the MLS data [12], because it is easy to control the trajectory of the sensor in order to collect complete data of the power line components.

Narrow vertical objects such as power line poles are not always well visible in the ALS data [4], especially if the flight path of the platform is straight on top of the power line. However, poles can easily be distinguished from the MLS points clouds (Fig. 3). Also, the studies on the detection of general vertical pole-like objects from the MLS data have reported good results (see, e.g., [10,36]). Detailed modeling of pole-like objects from the MLS data could be utilized, for example, to create more accurate fragility models for utility poles [52]. The ratio of the tree height to the diameter of the trunk defines how easily the tree bends, for example, due to snow load. For the trees that are near the power line, MLS can estimate both of these tree attributes accurately [38], which is not necessarily true for ALS. This together with the MLS-based accurate mapping of below canopy structures can be used to reveal trees, or parts of a canopy thereof, that are in danger of falling across the power line, for example, by accumulated snow.

Typically, cameras are incorporated into the MLS systems and the image data can be used to model and monitor the state of the power line components, such as insulators [44]. MLS would be an ideal choice to collect up to date information on the power lines and possible damages, which would be of high value after a natural disaster, such as a storm. The MLS data can be collected with clearly lower efforts than what is required for shooting an ALS campaign, and flying restricted areas and moderate wind cause no problems.

2.2. Related work and the novelty of the current algorithm

Power line mapping from ALS point clouds has been studied in, for example, [6,13,18,26,30,41,42,57]. The methods typically consist of a detection phase, where power line points are separated from the other laser points, which is followed by a reconstruction phase, in which points belonging to individual power lines are identified and the 3D shape of the power lines is modelled. Different studies have treated the different stages to various extents.

Typical approaches for the power line detection include line detection (e.g., [6,42]), analysis of the point cloud structure (e.g., [41]), and classification using various features (e.g., [13,18,30]). In practice, combinations of different approaches have been used in many studies. Typical features used in the classification include the return intensity, the difference between the first and the last pulse heights, and the features describing the spatial distribution of the points. Machine learning algorithms and increasing numbers of features have been used in recent studies [18,30].

The reconstruction methods typically begin with candidate power line points found in the detection stage. Then the methods proceed with a geometric modeling of the power line. Iterative and piecewise growing approaches have been presented [26,41]. The main idea is to first define local models and then to refine them to achieve final and complete catenary curve models.

ALS methods cannot directly be applied to the MLS data. For example, some existing ALS methods utilize the intensity of the returning laser pulse or the height difference between the last and first pulses. The intensity of the returning laser pulse is low for the power lines in the airborne data, because the footprint of the laser beam is large compared to the width of the conductor. However, the footprint of the MLS is considerably smaller than that of the ALS. Therefore, consistent intensity difference between the power lines and larger objects is not observed in the MLS data. In addition, difference between the first and last pulse (if applicable at all) is not a good feature as the ground is not seen with the same pulses that see the power lines.

Power line component mapping using the MLS data has been studied in [12,17,29,56]. All studies have concentrated on urban or road environments in which the data has been collected using wheeled platforms based on road network.

Kim and Medioni [29] extracted power lines and poles from a combined ALS and MLS point cloud. First, they removed the ground and the buildings and then extracted the points whose local neighborhood was situated approximately on a line in 3D space (linear points from now on) using tensor voting. The power lines and the poles were retrieved from the linear points using surface growing. When growing the power lines, they used only the linear points whose first principal component was close to horizontal (power line candidate points); when growing the poles, the direction was close to vertical. In addition, the power lines were grown only from the points that had a large enough height difference compared to the ground level.

Cheng et al. [12] classified and reconstructed power lines using the MLS point clouds. First, they classified power line candidate points based on the height above the ground level, up-down continuity (points with empty space on top of and below them), a linearity measure similar to Kim and Medioni [29], and the point density. Then they extracted lines in the horizontal plane using Hough transform, a voting method, which can be used to detect parametric shapes [14,20]. The power lines were reconstructed using surface growing, surface patch merging, and a second order curve fitting.

Guan et al. [17] extracted and reconstructed the power lines, the poles and the towers from distribution and transmission lines using the MLS data. First they classified the power line pole and the power line candidate points using the height above the ground level and the point density. Then, similar to Cheng et al. [12], they extracted horizontal lines from the power line candidates using Hough transform. Guan et al. [17] reconstructed the power lines using connected component labeling and catenary curve fitting methods. The towers and the poles were recognized by first segmenting the pole and tower candidate points and then classifying the segments based on the segment size and shape.

Yadav and Chousalkar [56] classified and reconstructed power lines from the MLS point clouds. First, they classified power line candidate points based on the point's height with respect to the ground level using a two-dimensional (2D) gridding. Second, based on 2D point density, they removed vegetation and building points. Third, they extracted lines in the horizontal plane using the Hough transform. Fourth, they segmented single power lines and performed a second order curve fitting to fill gaps and to reconstruct the power lines in 3D.

The algorithm developed in this study extracted the horizontal locations of the power lines. The power lines were retrieved from the candidate points as connected line segments. In the power line pole extraction, we used the same basic principles as in Kim and Medioni [29]. The power line extraction method contained the same two basic phases as previous methods developed for the MLS point clouds, that is, power line candidate point extraction followed by a retrieval of power lines from the candidates. We classified the power line candidate points in the same way as Kim and Medioni [29] and after that we used a voting-based method similar to Cheng et al. [12], Guan et al. [17], and Yadav and Chousalkar [56], to find horizontal lines from the candidates. The linearity measure that we used in the candidate point classification was the same used in [37], which is different to the methods of Kim and Medioni [29] and Cheng et al. [12]. Instead of Hough transform, we used random sample consensus (Ransac) [15] to find the horizontal lines. Ransac is another type of voting method that can be used, for example, to detect shapes from point clouds [9,11,51]. Because voting methods do not guarantee connectedness, the lines found

using Ransac were segmented to retrieve connected power line segments, which provided the horizontal locations of the power lines. However, if the basic 2D connected component (CC) labeling was applied (as in [17]) the connectedness criterion had to be rather loose due to the large (even several meters long) gaps in the point cloud along the power lines. The filling of the large gaps resulted in false detections, for example, from the forest. To remove the false detections, a novel segmentation method, called connected power line search (CPLS) was developed. CPLS utilizes the knowledge of the 3D shape of the power lines. It is based on 2D CC labeling to which a smoothness constraint is added, which takes into account the 3D shape of the power lines by using also the z-coordinates of the points. CPLS was able to retrieve the power lines and at the same time remove false detections, which the original 2D CC labeling produced.

The novelty of our method lies in the way we remove false detections using the novel CPLS method. Our goal was not to reconstruct the power lines in 3D as in Guan et al. [17], Cheng et al. [12], and Yadav and Chousalkar [56], but to find their horizontal locations. However, CPLS method utilizes also the z-coordinates of the point cloud to remove false detections.

3. Data and equipment

3.1. The study area and data collection

The study area was situated in a rural district in Loviisa in Southern Finland, and it contained forest and arable land (Fig. 1). The power line corridor under study was situated almost totally outside the road network, and it contained a 20-kV power line with wooden poles (Fig. 2).

The laser scanner data was collected with an all-terrain vehicle (ATV) and by a person with a backpack to which the scanner was installed (PLS). The laser scanner was a phase-based Faro Focus^{3D} 120S, which is originally a static 3D terrestrial laser scanner. However, in this study the scanner was set on a profiling mode, where it scans close to vertical cross-track 2D profiles of 305° field of view. In practice the scan profiles are tilted forward to about 15–20° on the backpack and slightly less on the ATV, but natural variation occurs due to terrain especially for the ATV setup. The movement of the platform (ATV or a person), tracked by the NovAtel SPAN Flexpak6 + UIMU-LCI GNSS-IMU positioning, gives the third dimension for reconstructing the scene in 3D. The IMU (inertial measurement unit), is used, for example, to measure

Fig. 2. A photograph from the test site. The operator with the backpack laser scanner can be seen under the power line.

the rotations of the platform. The data collection was carried out at a 95-Hz scan frequency and 488-kHz point measurement rate with 200-Hz position and attitude data from the GNSS-IMU. The angular accuracy of the post-processed GNSS-IMU solution is estimated to be even after 60 s GNSS outage 0.006°, 0.006° and 0.010° in roll, pitch and heading, respectively. Scanner angular accuracy is estimated conservatively to be 0.005°. This results in an approximate 14-mm positional point uncertainty at 50-m range from the scanner.

Fig. 1 shows the trajectories of the two platforms during the data collection superimposed on an aerial ortho image. In an open field area with smooth terrain, the ATV is able to achieve clearly higher speed than a walking person and thus it is preferred due to its efficiency (number of kilometers of power line per hour). However, as the terrain becomes rougher, especially in the forest, the PLS may become more efficient as the terrain roughness, rocks, and other obstacles slow down the ATV substantially. Therefore, the ATV trajectory was situated mostly in the open field areas and the PLS trajectory only in forested areas. An example of a point cloud collected using the backpack can be found in the Fig. 3.

The one-dimensional (1D) point density along the power line (hereinafter along-the-line point density) varied from approximately 15 points/m in the open field to hundreds of points/m in the forest. For the given scan parameters the angular resolution in a profile was 1.2 mrad, that is, 12 mm point spacing at 10 m distance from the scanner.

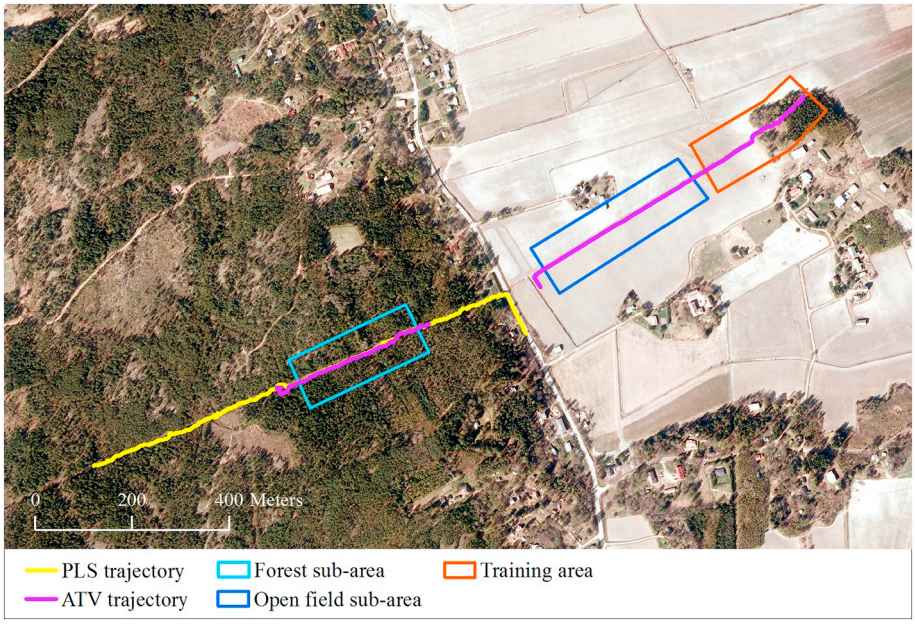

Fig. 1. An aerial view of the study area. Ortho image © National Land Survey of Finland 2011. Polygons depict the training area (orange) and the two sub-areas inside test area that are the forest sub-area (cyan) and open field sub-area (blue). The trajectories outside the training area compose the test area. Yellow line corresponds to the PLS trajectory and magenta line to the ATV trajectory.

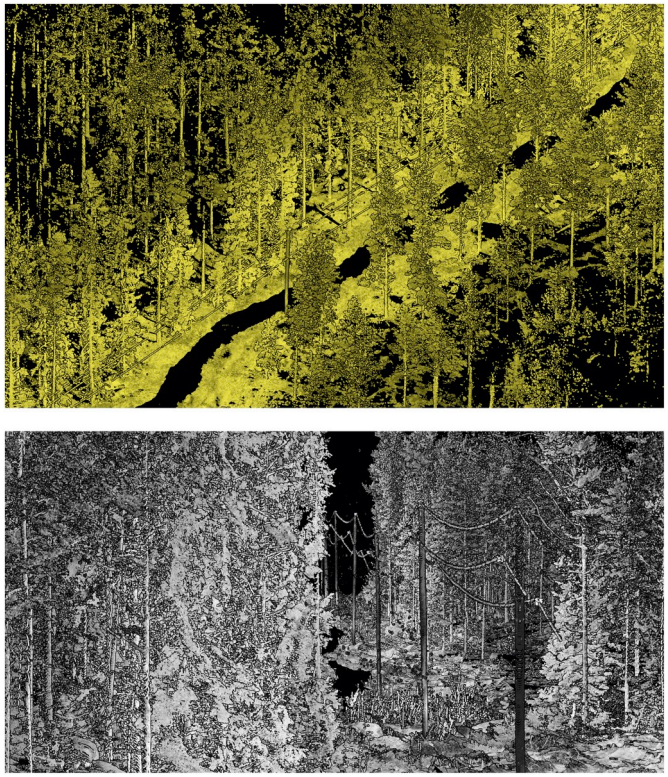

Fig. 3. Two views to the MLS point clouds in the study area. The shade of the points is defined by the return intensity of the echoes. A black area in the middle corresponds to a 55° dead angle in the scanner field of view along the trajectory. For color illustration of the top figure, the reader is referred to the online version of the article.

The study area was divided into a training and test part (Fig. 1). The training set (area) consisted of approximately 260 m of power line corridor that was scanned with an ATV and contained both forest and open field (Fig. 1). The test set consisted of the remaining part of the study area. It contained approximately 770 m of power line scanned with an ATV (ATV test set from now on) and 1065 m power line scanned using a backpack scanner (PLS test set). The ATV test set contained both forest and open field areas and the PLS test set, in practice, only forest areas. The point densities along the power lines varied similarly in the training and test sets.

The training area was used to tune the parameters of the developed algorithms, whereas the test area was used to evaluate the accuracy of the developed methods. The purpose of using separate training and test sets was to avoid overfitting of the parameters to the data, which was used to evaluate the accuracy of the algorithms.

In addition, two sub-areas were selected inside the test area (Fig. 1). The first sub-area was situated in forest and it was scanned with both the ATV and the backpack. The forest sub-area was used to investigate how the automatic power line extraction works using the PLS compared to using the ATV in the same area. The second sub-area was located in the open field and it was scanned only with the ATV. The open field sub-area was used together with the forest sub-area to compare the performance of the automatic power line extraction in these two land cover types.

3.2. The challenges of the mobile laser scanning technology in the power line corridors outside the road network

Though kinematic approach provides with a reasonable and fast way of completing corridor mapping tasks, the MLS technology possesses some challenges that need to be addressed. The major issue in forested areas is that the power line corridor is often surrounded by tall trees, which may block the GNSS signals hampering the positioning. Due to the loss of signals, the accuracy of the positioning system deteriorates and the estimated position may drift severely. Typically, the GNSS-IMU-positioning has been found to maintain better than 1 meter horizontal accuracy in boreal forests, while the elevation may drift more drastically, and is known to be the most uncertain direction to determine with GNSS in general [28]. The drifting of the GNSS-IMU solution may be compensated by applying simultaneous localization and mapping (SLAM) [35]. However, combination of SLAM and MLS in a forest environment is a rather new research topic, and thus SLAM was not applied in this study. In the data set used in this study, the maximum horizontal drift in a 50-m-long power line was approximately 10 cm in the forest and in good GNSS conditions.

In rural areas, outside the road environment, the terrain is often rugged in the power line corridor (e.g., forest). Therefore, the platform speed (walking or ATV) is often slow and sometimes stalled due to unavoidable stops and rerouting. The low platform speed results in condensations of points in the point cloud, which may be challenging for the automatic point cloud processing algorithms. For example, condensations of adjacent scan lines during a stop may create features in the point cloud that are similar to those of power lines. Therefore, we removed points, which were collected when the 3D speed of the platform was < 2.5 cm/s, because then the platform was standing still effectively. Also, typically the accuracy of the GNSS positioning sensor attitude deteriorates when the platform speed is slow, resulting in a noisy appearance of the power lines in the point cloud.

3.3. Data pre-processing

After the data collection, the raw laser scanning data was georeferenced into a 3D point cloud using the post-processed trajectory data. The data was projected to ETRS-TM35FIN map coordinate system, and the point elevations were in ellipsoidal heights. Then the point cloud was filtered to remove stray points falsely appearing in the air.

After removing the points collected during a low platform speed (< 2.5 cm/s), most of the ground points were removed using the same principles as in [37]. The ground extraction method is based on finding smooth nearly horizontal surfaces from the point cloud using local surface planarity measures, surface growing, and surface patch merging. As the MLS platform was moving rather close to the power line, it was possible to remove the points whose horizontal distance to the trajectory of the scanner was > 20 m without losing any power line points. This limited the search space in the following power line extraction, which in turn decreased the computation times and lowered the probability of incorrect detections from the surrounding environment.

4. Algorithms

The input to the power line and pole extraction algorithms was the pre-processed point clouds (see Section 3.3). We assumed in all phases of the algorithms that the power lines' slope is $\leq 45°$. This is a valid assumption in our test area, which contains no steep slopes. In more hilly terrains (e.g., mountains), higher values may be needed. First, we extracted power line candidate points and then we retrieved power lines from the candidates. Poles were extracted after the power line retrieval. A flowchart of the power line and pole extraction algorithms can be found in Fig. 4. Pseudocode of the power line extraction algorithm can be found in the Appendix B. The selection of the values of the parameters of the algorithm is described at the end of each section for the most part. For some parameters, it was difficult to choose their values using general power line properties. Therefore, we selected their values using a grid search and a separate training data set (see Section 5.2).

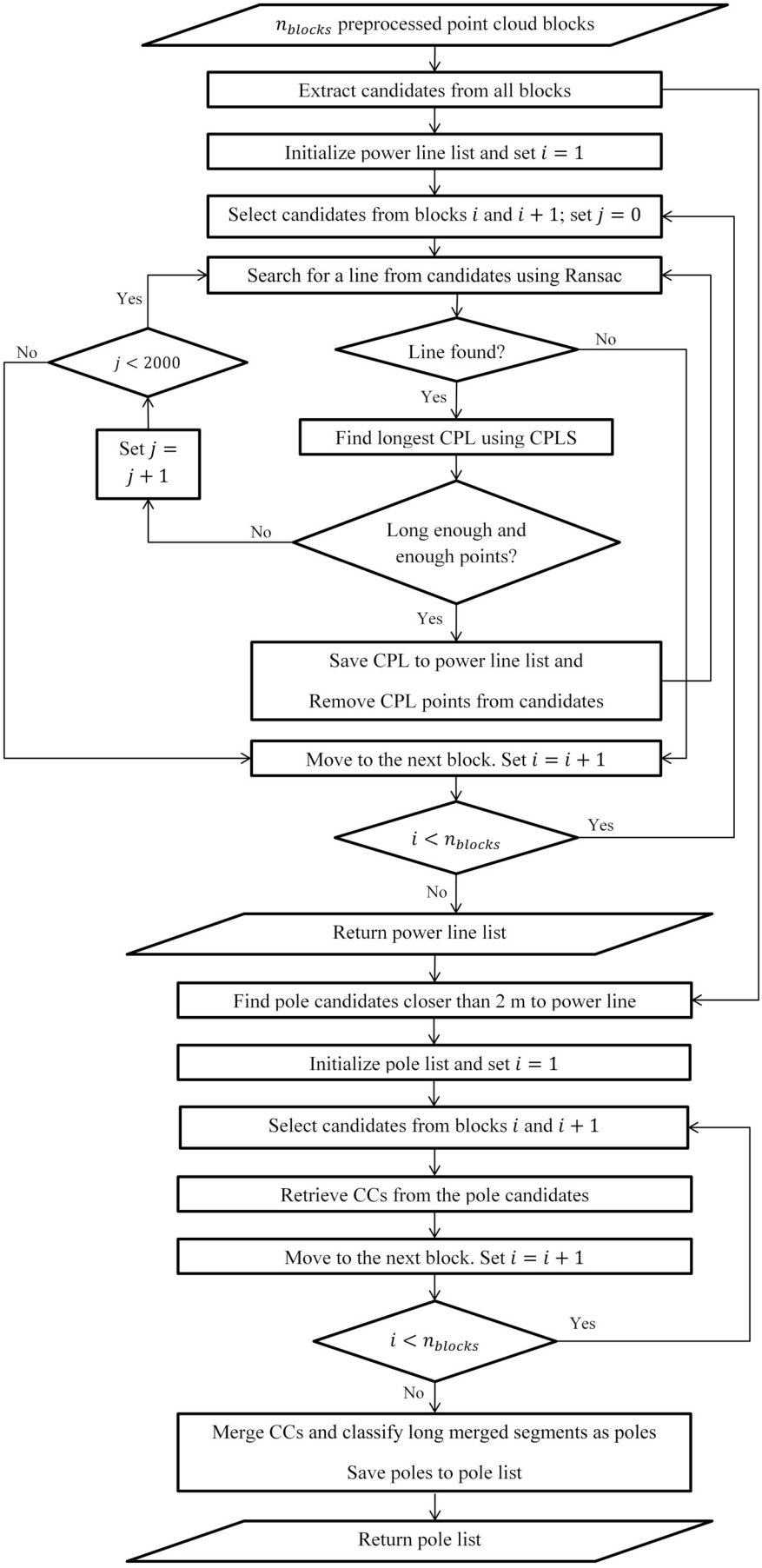

(caption on next page)

Fig. 4. A flowchart of the power line and pole extraction algorithms. n_{blocks} is the number of the point cloud blocks, i is the index of the point cloud block, CPL stands for connected power line (i.e., a connected line segment classified as a power line), CPLS stands for CPL search, j is the number of consecutive calls of Ransac without finding a power line, and CC stands for connected component. Pseudocode of the power line extraction algorithm can be found in the Appendix B.

4.1. Block-wise processing

During the data collection, the MLS data was divided into blocks of approximately 6–15 million points and with length of 20–170 m along the power line, depending on the platform speed and the amount of vegetation around the power line corridor. Construction of the voxel structure (Section 4.2) is the most computationally and memory intensive phase of the method, and it is much more efficient to construct the voxel structure in smaller blocks than for the whole data set at once. Also, Ransac is more efficient and reliable when it is performed locally.

Therefore, we extracted power line candidate points from each block separately. However, the edges of the point cloud blocks cause problems, especially if the direction of the power line changes close to the edge. Then the remaining part of the line on the edge has to be detected separately from the rest of the line because the lines are not parallel. If the nonparallel section on the edge is shorter than the minimum length of the line segment, the section cannot be detected (Fig. 6(b)). Even if the power line does not change its direction, the power lines may still be missed close to the edge because the extracted lines may not be exactly parallel to the power lines.

To overcome these challenges, the power lines were retrieved from the candidates of two consecutive blocks at a time, that is, from first and second block, from second and third block, etc. In this way, each block was processed twice in the conductor retrieval and, thus, the same power line was typically detected more than once. However, the line segments can be merged at post-processing to form unique power line segments, but this was out of the scope of this study as we were interested to find the 2D locations of the power lines.

4.2. The extraction of the power line candidate points

Points corresponding to power lines have a local neighborhood in which all points lie approximately on a line. Such points are referred to as linear points in the following and they were classified using the principal component analysis (PCA) (see, e.g., [23]). PCA gives the directions of the highest variances, that is, principal components (PCs) and the corresponding variances of a set of points. First PC corresponds to the direction of the line that best fits to the point set using a least squares criterion [8]. Let $\lambda_1 \geq \lambda_2 \geq \lambda_3$ be the variances corresponding to the first, second and third PC of a point set. If the highest variance λ_1 explains most of the total variance $\sum_{i=1}^{3} \lambda_i$, the points are situated approximately on a line. Therefore, we used a linearity measure L [37] to classify linear points with an equation $L = \lambda_1/(\sum_{i=1}^{3} \lambda_i)$. If the linearity L of a point was above a threshold, the point was classified as linear. We used a threshold value of 0.9 for L, which was selected based on the grid search and previous experience. We also assumed that the power line's slope is not $> 45^\circ$ and hence linear points, whose first PC was sloped more than this were removed. The remaining linear points were selected as candidates, which were used in the next phases of the algorithm to find power lines.

To hasten processing, the point cloud was divided into a regular voxel structure similarly as in [37], and with a voxel size of 30 cm. The linearity L was calculated for each voxel by performing the PCA for the points inside the 26-neighborhood of the voxel. Each voxel was classified as linear or nonlinear based on L and points inside the linear voxels were labeled as linear.

The voxel size should be selected based on four criteria: 1) the distance between two neighboring power lines, 2) the distance between the power lines and other objects, 3) along-the-line point density, and 4) reliability of the power line candidate point extraction. The neighborhood of a power line voxel should not contain any other points than neighboring points on the same power line; otherwise the point is not necessarily classified as linear (criteria 1 and 2). The 26-neighborhood should contain at least 3 points in order to decide whether they lie along a line. The along-the-line point density of the MLS data of this study was > 15 points per meter. If the voxel size was > 10 cm, the 26-neighborhood would always contain 4 points or more; therefore 10 cm can be considered as a practical lower limit for the voxel size (criterion 3). However, based on preliminary tests, the use of voxel size smaller than 20 cm would result in too many non-power line candidate points (criterion 4). Taking into account the distance between two neighboring power lines, 30 cm was a practical upper limit for the voxel size (criterion 1). It was not clear which voxel size, 20 cm or 30 cm, would result in the most reliable candidate point extraction results (criterion 4). Therefore, we selected the voxel size using the grid search.

4.3. The retrieval of the power lines

The power lines were extracted as connected line segments from the candidate (linear) points (Fig. 4). First, a line was searched for from the candidate points in the horizontal plane using random sample consensus (Ransac) [15]. Ransac is a method that can be used, for example, to detect shapes such as spheres and cylinders from point clouds by random sampling [9,11,51]. In this study, Ransac was used to detect lines from a 2D point cloud in the horizontal plane in the following way. First, two points were selected randomly and a line was fitted to them. Then inliers, that is, all points whose normal distance to the line was < 10 cm were retrieved. If the number of inliers exceeded a threshold value of 100 points, the inliers were classified as points that belong to a same line, and the line detection was considered successful and finished. If the number of inliers was less than the threshold, a new line was searched for from the point cloud as above by selecting new point pair randomly. New point pairs were sampled until a line was detected or until a maximum number of iterations m was reached, where m is sufficiently large number. Even though Ransac was applied in the horizontal plane, also the z-coordinates of the points were preserved in the line detection process in order to use them in the CPLS method later.

After a line had been detected using Ransac, connected segments were searched for from the line using the developed CPLS method that takes into account the 3D shape of the power lines (see Section 4.3.1). The longest connected segment was retrieved and if it was longer than 20 m and contained > 100 points, it was classified as a power line. Points belonging to the segment were removed from the list of power line candidate points.

Next, a new power line segment was searched for from the remaining candidate points using the same procedure. The procedure was repeated until no acceptable connected line segment was found in 2000 consecutive calls of Ransac or if Ransac did not find a line.

The maximum normal distance to the line for the inliers (10 cm) was selected based on the grid search. 10 cm was also the maximum horizontal drift along a 50-m-long power line in good GNSS conditions in the forest (see Section 3.2). The minimum length of a power line segment (20 m) was set based on the grid search. The minimum number of points in the power line (100 points) was set rather low in order to find conductors also in areas of low point density. The threshold for the number of inliers in Ransac (100 points) was set equal to the minimum number of points in a power line. The maximum number of iterations m inside Ransac determines the reliability of line detection; the greater m is the higher the probability that all lines in the point cloud are detected. Higher value of m means also more computation. It can be shown that m can be chosen in such a way that the probability of

detecting a line is greater than or equal to some fixed value (see Appendix A). Therefore, we fixed the lower limit for the probability of detecting a line to a value of 0.9 and based on that we calculated m. The lower limit of 0.9 was chosen based on a balance between computational complexity and reliability of detecting a line. The minimum size of a line needed in the calculation of m (Appendix A) was set equal to the inlier threshold of 100 points. Various values were tested for the maximum number of consecutive Ransac calls without a found power line segment and 2000 repetitions was found to be enough.

4.3.1. Connected power line search (CPLS) method

As Ransac does not guarantee point connectedness along the line, a connected segment is usually searched for from the points on the line using, for example, connected component (CC) labeling (see, e.g., [50]). However, the application of the basic version of the CC labeling exhibited also segments that were not power lines, for example, from candidate points found from the forest. Therefore, we developed a modified version of the basic algorithm that also takes into account the 3D shape of the power lines. We call the developed method 'connected power line search' (CPLS). A pseudocode of the CPLS algorithm can be found in Appendix B (Algorithm B.2).

CPLS from the points that lay on the line detected by Ransac started by ordering the points along the line. The first point on the line was selected as a seed for the first segment and the seed was compared to the next n_{window} points on the line. Those of the next n_{window} points, which satisfied the following two conditions were added to the segment: 1) the horizontal distance to the seed point was below 4 m and 2) the slope of the line joining the point and the seed was $< 45^{\circ}$, that is, the maximum assumed slope of a power line. Next, the last point of the segment was retrieved and it was compared again to the next n_{window} points on the Ransac line; new points were added to the segment using the same criteria (1–2) as above. This procedure continued until no new points that satisfied the conditions (1–2) were found on the Ransac line. Next, a new segment was initialized by selecting the first point from the set of Ransac line points that did not belong to any segment yet. This point was set as a seed and the segment was grown similarly as above. New segments were searched for until all points on the Ransac line belonged to some segment. Noise in the coordinates of the points may cause large angles between nearby points. Therefore, the angle criterion (2) was ignored if the points were < 10 cm apart.

The maximum horizontal distance to the last point (or seed point) of the segment (4 m, criterion 1 above) in the connected segment search was selected based on the grid search. For the size of the search window n_{window}, 30 points was found to be large enough value based of testing.

4.4. The extraction of the power line poles

The extraction of the wooden poles of the power line (poles hereinafter) consisted of four phases. First pole candidates, that is, linear voxels (see Section 4.2) which were closer than 2 m to the extracted power lines were retrieved. As the poles are nearly vertical structures, it was also demanded that the angle between the candidates' first PC and vertical direction was $< 45^{\circ}$. Second, CCs were retrieved from the pole candidates using the 26-neighborhood as a connectedness criterion as in Lehtomäki et al. [37]. These two phases were performed for all pairs of adjacent data blocks. Third, all found segments, that is, CCs from all pairs of blocks were merged using the pole merging algorithm of Lehtomäki et al. [36]. In the merging algorithm, two segments were merged if the gap between them along the main axis (first PC) of the longer segment was < 1 m and if the center of mass of the shorter segment was < 5 cm apart from the main axis of the longer segment. Finally, all merged segments, which were longer than 2 m were classified as poles.

Poles were extracted after the power lines in order to retrieve less false detections. If pole detection had been performed before power line extraction a considerable number of tree trunks would have been detected as poles. However, the shape of the power lines (long linear structures) is such that they are rarely found from the forest. Therefore, the extracted power lines can be used to limit the search space in the pole extraction.

All parameter values of the pole extraction were selected using the grid search. The results were found not to be sensitive to the maximum angle of the voxel's first PC and vertical direction. Often, the supporting poles are at least in 30° angle with respect to the vertical direction. To be able to retrieve all these structures, we selected the largest value of the grid (45°).

5. Results and discussion

5.1. Reference collection and accuracy evaluation

All power lines and wooden poles were collected manually from the point clouds to be used as a reference in the evaluation of the accuracy of the methods. The power lines were collected as 2D line segments between the end points of spans (two consecutive poles). For each pole, the 2D location was collected.

The accuracy of the power line extraction was evaluated point-wise by sampling the reference lines (RLs) and extracted lines (ELs) uniformly. An RL sample point was marked as 'found' if at least one EL sample point lay within a 10-cm range from it; otherwise the RL point was marked as 'missed'. 10 cm was used as an acceptable error tolerance, because it was the maximum horizontal drift in a 50-m-long power line in the forest and in good GNSS conditions (see Section 3.2). The recall was defined as the ratio of number of found RL samples to the number of all RL samples. Recall was evaluated by sampling the RLs in 1 m and ELs in 1 cm intervals. An EL sample point was marked as 'true positive' if at least one RL sample point lay closer than 10 cm from it; otherwise it was marked as 'false positive'. The precision was defined as the ratio of number of true positive samples to the number of all EL samples. Precision was evaluated by sampling the ELs in 1-m and RLs in 1-cm intervals.

The accuracy of the pole extraction was evaluated by comparing the center points of the extracted poles to the locations of the reference poles in the horizontal plane. A reference pole was marked as found if a detected pole was found within 0.5 m from it; otherwise the reference was marked as missed. The corresponding extracted pole was marked as true positive. The recall of pole extraction was defined as the ratio of number of found reference poles to the number of all reference poles. The precision was defined as the ratio of number of true positive poles to the number of all extracted poles.

Because Ransac contains random sampling, the outputs of the algorithms vary from one repetition to another. Therefore, the precision and recall are random variables. To gain results which describe how the algorithm works on average, we repeated the power line extraction 100 times with the test set. In the parameter tuning (see Section 5.2) the number of repetitions had to be limited to 10 with the training set, because of the large number of repetitions needed in the tuning.

5.2. Parameter selection

The values of most of the parameters of the power line extraction algorithm were selected using prior knowledge of the characteristics of the power lines. However, some parameters were such that their values were difficult to select using only prior knowledge. Also, some parameters were dependent on each other, that is, their optimal values depended on the values of other parameters. Therefore, we used a separate training data set (see Section 3.1) and a d-dimensional grid search to select the values of these parameters, where d is the number of the parameters.

Grid search is a brute-force method (also called exhaustive search) to optimize parameters by evaluating the objective function in a regular grid [21,47]. The grid dimensions correspond to the parameters to be

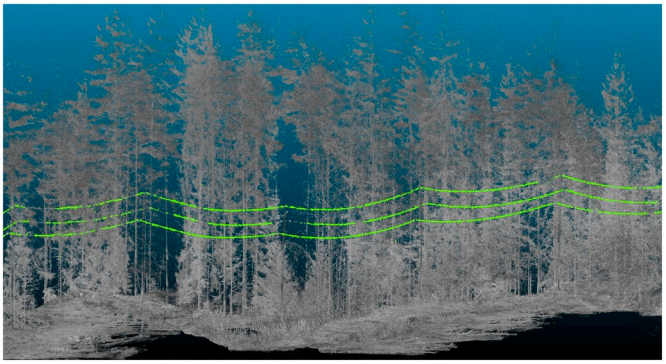

Fig. 5. The point cloud (shades of gray) and the extracted power line points (green).

optimized and each grid vertex corresponds to one parameter value combination. The objective function is evaluated at each vertex and the vertex (parameter value combination), which gives the highest value for the objective function is selected as optimal. In this study, the objective function was the mean of the precision and recall which was further averaged over the 10 repetitions (see Section 5.1).

First, five parameters of the power line extraction were tuned in a 5D grid. Then they were fixed to the optimal values and five pole extraction parameters were tuned in another 5D grid. The power line extraction parameters were (grid vertex values inside brackets; all units in meters except for the dimensionless quantities or if stated otherwise) the voxel size (0.2, 0.3), the minimum length of a connected line segment (10, 20, 30, 40), the maximum distance in CC labeling (2, 4, …, 10), the threshold for the linearity measure (0.9, 0.95), and the upper limit for the normal distance to the line for the inliers of Ransac (0.05, 0.1). The five pole extraction parameters that were tuned using the grid search were the maximum horizontal normal distance to the power line (1, 2, 4, 6), the minimum height of a pole (1, 2, …,7), the maximum gap in a pole (1, 2, 3), the maximum distance between the poles' axes in the merging (0.05, 0.1, 0.2), and the maximum angle between the first PC of vertical voxels and the z-axis in degrees (15, 30, 45). The values of the grid vertices were selected based on prior knowledge and preliminary tests.

Based on the grid search, the voxel size was set to 30 cm, the minimum length of a connected line segment to 20 m, the maximum distance in CC labeling to 4 m, the threshold for the linearity measure to 0.9, and the upper limit for the normal distance to the line for the inliers of Ransac to 10 cm. In the pole extraction, the maximum horizontal normal distance to the power line was set to 2 m, the minimum height of a pole to 2 m, the maximum gap in a pole to 1 m, the maximum distance between the poles' axes in the merging to 0.05 m, and the maximum angle between the first PC of vertical voxels and the z-axis to 45°.

Using the optimal parameter settings gained from the grid search, the recall of power line extraction with the training set was 98.8%; the corresponding precision was 96.2%. The selection of grid vertex values for the voxel size is explained in Section 4.2. If voxel size had been 20 cm instead of 30 cm, the average recall would have been 1 percentage point lower but the precision would have remained the same. However, the maximum distance in CC labeling needed to be changed into 2 m in order to achieve this accuracy. If one wants to achieve the same recall with a 20-cm voxel size as with the 30-cm voxel size by tuning the other parameters, the precision would be as low as 93% or less. A 2-m maximum distance in CC labeling would have resulted in a 1-percentage-point decrease in the recall, but then one must have used a 20-cm voxel size. If the maximum distance of the CC labeling had been changed into 6 m, 8 m, or 10 m the accuracies would have been at least 2 percentage points lower. Based on preliminary tests, the use of lower linearity threshold than 0.9 did not provide more power line candidate points in practice. If the linearity threshold had been 0.95, the recall would have decreased 0.8 percentage points. We have used a threshold of 0.9 for the linearity also in other applications successfully to classify linear elongated shapes (see, e.g., [37]). Using 10 m as a minimum length of a connected line segment would have decreased recall < 0.5 and precision > 1 percentage point. If the minimum length was 20 m or higher, the parameter could be used to find a suitable application-specific balance between precision and recall. When the minimum length was 40 m, the precision was as high as 98.7% while the recall was 94.0%. Based on our objective function, best balance was found using 20 m. If the upper limit for the normal distance to the line for the inliers of Ransac had been set to 5 cm, recall would have decreased 1 percentage point. 10 cm was justified also by the fact that the maximum horizontal drift in a 50-m-long power line was approximately 10 cm in the forest and in good GNSS conditions.

Table 1
The results of the extraction of the power lines in the test set. The results are from the 100 repetitions of the power line extraction. The standard deviations over the repetitions were less than 1 percentage point in all cases.

Platform and area	Mean recall of power line extraction (%)	Mean precision of power line extraction (%)
Test set (ATV + PLS)	93.3	93.6
ATV test set	93.6	95.5
PLS test set	93.1	92.3
PLS forest	98.8	93.2
ATV open field	99.9	97.4
ATV forest	97.7	93.7

5.3. Power line extraction results

A view to the point cloud with extracted power lines highlighted can be found in Fig. 5. The results of the accuracy evaluation of the power line extraction in the test set are listed in Table 1. The table lists the average recalls and precisions over the 100 repetitions separately for the PLS and the ATV point clouds and the forest and open field sub-areas. In the evaluation of the combined test set (ATV + PLS), the ATV and PLS test sets were treated as if they were two separate areas. The standard deviations of the samples over the 100 repetitions were less than 1 percentage point in all cases.

The recalls in the PLS and the ATV test sets were very close to each other (less than 1 standard deviation over the 100 repetitions) but the recall in the ATV test set was slightly higher. However, the precision in the PLS test set was clearly lower (3.2 percentage points) than in the ATV test set.

In the forest sub-area, the recall of the PLS was 1.1 percentage points higher than that of the ATV, which is more than the standard deviation, and thus somewhat significant. However, the difference can probably be explained by the stray points around the power lines in the ATV forest sub-area (see Section 5.4). The precisions were similar between the PLS and ATV in the forest sub-area. Hence, there does not seem to be differences in the accuracies between the platforms.

A clearer difference can be seen between the ATV forest and the ATV open field sub-areas. In the open field, the recall and precision were 2.2 and 3.8 percentage points higher compared to forest.

The recalls of all sub-areas were clearly higher than those of the whole test sets (ATV or PLS). This was caused (by chance) by the selection of the sub-areas. Most of the missed reference power lines were situated close to the borders of the ATV test set, which were not part of the sub-areas. In addition, most of the missed reference power lines were outside the forest sub-area in the PLS test set.

We also performed a statistical analysis of the results to analyze how much the results varied between the repetitions. The 100 samples of the recall and precision of the power line extraction in the ATV test set, PLS test set, and the whole test set passed the Wilk-Shapiro test for

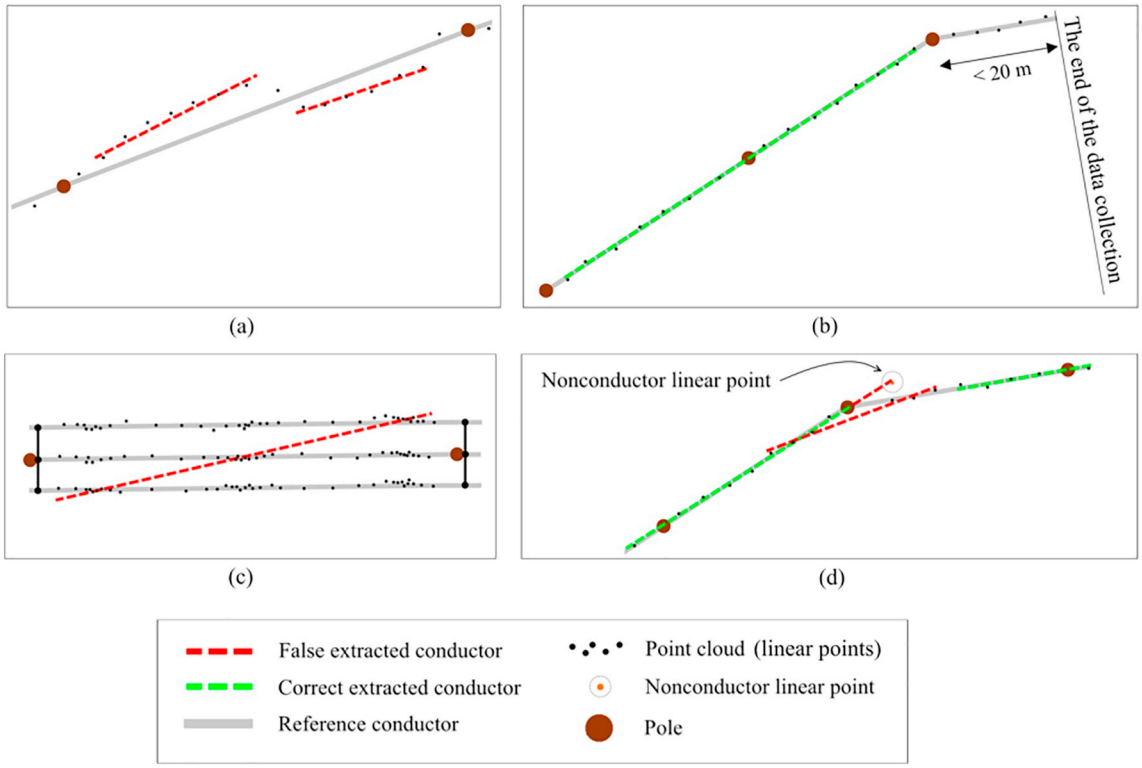

Fig. 6. Different causes for the errors in the power line extraction: (a) drifting of the positioning; (b) the edge of the point cloud; (c) heterogeneous along-the-line point density; (d) pole location and non-power line point classified as linear.

normality [48,49,53,55] with a significance level of 0.1. As also the standard deviations of the samples were less than 1 percentage point, it can be stated that the precision and recall of the power line extraction lay close to the mean value in all repetitions and the method is robust against the random sampling.

5.4. The error analysis of the power line extraction

The causes for the errors listed in this section are contributory, which means that there may have been two or more reasons for a particular error case. Therefore, the sum of the percentage points exceeds 100. We performed the error analysis by checking visually the results of several repetitions of the power line extraction from the test set. Therefore, the percentages provided in this section are estimates. The drifting of the positioning was the largest error source in the power line extraction; it was the cause for approximately 60–70% of all errors, including the missed reference power lines (omission errors) and the false power lines (commission errors). Because of the drifting, the power lines in the point clouds were not lines but curves that drifted around the reference and sometimes their distance to the reference was larger than 10 cm, thus causing omission and commission errors (Fig. 6(a)).

Other considerable causes for the omission errors were a poor visibility of the power lines in the point cloud (this caused approximately 40% of the omission errors), the edges of the point clouds (20%) (Fig. 6(b)), stray points around the power lines (10%), and that the power lines were inside tree branches (5%). The edges of the point cloud mean either the starting or ending points of the data collection or a branching line. If the direction of the power line changes close to the edge, the power lines may be missed there, because the branch or the non-parallel segment is shorter than the minimum length of the power line segment (see Section 4.1 and Fig. 6(b)). The stray points and tree branches around the power lines caused that the power line points were not classified as linear and the power lines were thus missed. Stray points caused errors only in the forest part of the ATV test set.

Other considerable causes for the commission errors were a heterogeneous along-the-line point density (approximately 40% of the commission errors were caused by this) (Fig. 6(c)), non-power line points classified as linear (20%), and pole locations (20%) (Fig. 6(d)). Especially in the forest, the velocity of the scanner was nonuniform, which caused condensations of points in the low-velocity locations. If Ransac samples candidate points on two or more locations where the along-the-line point density is high, the number of points on the line travelling through these locations could reach the threshold and a false line could be detected (Fig. 6(c)). In pole locations, the power line may change its direction. This can cause two types of commission errors (Fig. 6(d)). First, the extracted line may extend outside the reference line after the change of the direction due to a non-power line linear point. Second, the extracted segment can take a short cut in the pole location.

The heterogeneous along-the-line point density caused more commission errors in the PLS test set than in the ATV test set and was the main reason for the lower precision in the PLS test set compared to the ATV test set. The reason for the difference is that the velocity of the scanner varied more in the forest than in the open field. The PLS test set was almost entirely in the forest whereas approximately half of the ATV test set was in the open field.

Most of the commission errors were situated close to the power line. In the ATV test set only 6% and in the PLS test set only 10% of the commission errors came from the forest surrounding the power line.

5.5. Power line pole extraction results

The precision and recall of the extraction of the power line poles in the ATV test set were 5 and 6.5 percentage points higher, respectively, compared to the PLS test set (Table 2). As in the power line extraction, a probable reason for the differences was that half of the ATV test set was situated in the open field whereas the PLS test set was situated almost

Table 2
The results of the extraction of the power line poles in the test area. The results are from the 100 repetitions of the power line extraction. In total, the ATV test set contained 18 and the PLS test set 28 poles.

Platform	Mean recall of pole extraction (%)	Mean precision of pole extraction (%)
ATV	83.3	99.4
PLS	76.8	94.4
ATV + PLS	79.4	96.0

entirely in the forest. In the forest, GNSS outages caused problems. The precisions were clearly higher than the recalls (Table 2), which means that most of the errors were caused by the undetected poles and only small amount of false detections were retrieved.

In the pole extraction, the results varied more between the repetitions compared to the power line extraction. The recall was constant in the ATV test set over all repetitions, but the precisions in both test sets and the recall in the PLS test set varied 7–20 percentage points (maximum value minus minimum value) between the repetitions. The large variation is natural, because the number of poles was rather small (18 in the ATV and 28 in the PLS test set). For example, in the PLS test set, missing of even one pole caused already a decrease of 3.6 percentage points in the recall.

5.6. Discussion

5.6.1. The effect of platform and land cover type

The results suggest that the platform does not have a significant effect on the accuracy of the power line extraction: The PLS and the ATV produced similar accuracy when applied in the same area. Instead, the land cover type (forest/open field) seems to have much stronger effect. Especially the precision but also the recall were higher in the open field sub-area and the open field dominated ATV test set compared to the forest sub-area and the forest dominated PLS test set, respectively. The precision was lower in the forest mainly because the along-the-line point density was inhomogeneous there due to the varying platform velocity.

5.6.2. The main error sources and suggestions for future actions

In all areas, the reason for most omission and commission errors was the drifting of the positioning solution of the scanner. In the forest, tall trees near the power line were a significant cause for the drifting, because they blocked the GNSS signal. This was also probably the main cause for the lower recall in the forest compared to the open field. As the edges of the point clouds caused a considerable amount of omission errors, they need to be taken into account in the planning of the data collection or post-processing of the data. The data collection should extend far enough outside the area of interest or the edges should be checked manually during the data processing.

In one location, the ATV had to deviate from the power line corridor and drove into the forest. This was very clearly seen in the positioning solution, where especially the z-coordinate started to drift fast. This underlines the need to tackle the problem of weak GNSS signal due to trees in future studies [35].

5.6.3. Pole detection

Even though the recalls of pole extraction were clearly lower than those of the power line extraction, MLS seems a promising technology also for the pole extraction. The pole detection method used in this study was based on rather simple principles and improvements in the detection accuracy can be assumed when a more sophisticated method is developed.

5.6.4. Comparison to previous studies

Previous studies on the extraction of power lines using the MLS data have concentrated on urban or road environments and, therefore, it is challenging to compare our results to those of the previous studies. Also, the differences in the measuring equipment, data quality, properties of the test sites (e.g., number of power lines), and the differences in the algorithm outputs (e.g., 2D locations of the power lines vs. reconstructed 3D power lines) make the comparison even harder. Yadav and Chousalkar [56] reported recall (completeness) of 91% and precision (correctness) of 99% in the power line extraction in a road environment (urban, peri-urban and rural). In the urban environment, Guan et al. [17] reported recall and precision values of 92% and 99%, respectively, in the power line extraction, and Cheng et al. [12] reported a recall of 94% and a precision of 99%. The recall of our method falls between the recalls of the studies listed above and is therefore in line with the previous results. However, the precision of our method is 5–6 percentage points lower compared to the previous studies. In our study, most of the commission errors were caused by the inhomogeneous along-the-line point density and the drifting of the positioning. These were not reported in [56,17,12], even though the GNSS signal may be weak in urban canyons [16,31,45]. In the urban and road environment, the terrain is smooth and the driving speed can be kept much steadier compared to the areas outside the road environment (e.g., forest). Consequently, the point density is more homogeneous and the positioning solution more accurate.

6. Conclusion

Aerial laser scanning (ALS or UAV) and land-based mobile laser scanning (MLS) are accurate remote sensing techniques that can be used to automate the inspection of the power lines, which has traditionally been labor intensive and subject to human errors. When the aerial inspection is impossible or unsafe, for example, due to regulations or weather conditions, MLS might be a good choice for the power line corridor inspection. In addition, MLS provides mapping information with a higher level of detail in the power line corridor due to the higher point density and 3D accuracy. In some cases, MLS could be a cheaper choice compared to the aerial inspection. MLS could also be used to fill gaps that remain after the aerial inspection. It is also usually easier to shoot an MLS campaign compared to an airborne one, if some area needs to be inspected urgently.

The application of the MLS to the power line mapping was studied in a rural environment outside the road network for the first time. In addition, a novel algorithm that automatically extracts the power lines from an MLS point cloud was developed and tested in a rural area, outside the road environment that contained both open field (arable land) and forest. Also, the extraction of the wooden power line poles was investigated using existing methods in the literature. Two different platforms, that is, a personal backpack and an all-terrain vehicle (ATV) were used to carry the scanning equipment.

The recall and precision of the automatic power line mapping were 93.3% and 93.6%, respectively. An extracted power line was considered correct if it was closer than 10 cm to the reference. The drifting of the positioning solution of the scanner was the largest (contributory) cause for the errors, causing 60–70% of all errors. The ATV and personal backpack platforms provided similar accuracy. However, the accuracy was higher in the open field compared to the forest. The differences were mainly caused by the inhomogeneous 1D point density along the power line and the weak GNSS signals in the forest.

The achieved accuracies are comparable to those of the previous studies in the urban and road environments, taking into account the differences between the areas inside and outside the road network. The results suggest that the accuracy of the power line mapping using MLS is enough for inspection purposes also outside the road environment.

In contrast to the airborne or UAV operations, the MLS approach avoids the need for paper work and experienced personnel in the data collection. Roughly speaking, the typical cost of the power line mapping is in the range of 100€/km in the European conditions. MLS is a feasible and cost-effective technology for the power line mapping if the daily inspection exceeds 15 km of power line, including the data processing. When using an ATV, data of > 100 km can be daily collected if moving inside the power line corridor

is easy enough and not limited too much by steep slopes or dense canopies. It is also easier and cheaper to multiply ground based systems than airborne units for improved data output. As with the ALS, when planning an MLS measurement campaign, the operator needs to take into consideration areas of limited access (e.g., the areas of the growing corn). Also, possible obstacles along the route (e.g., steep slopes, larger ditches, and rivers) need to be considered.

The extraction of the power lines and their catenary curves separately in each span was not treated in this study and will be a topic of a future study. In addition, the use of SLAM (simultaneous localization and mapping) [35] and related techniques, high density ALS data [40], and more accurate IMU (inertial measurement unit) to improve the accuracy of the georeferencing in case of a weak GNSS signal and rough terrain will be studied. The homogenization of the point distribution and the measurement of the distance between the vegetation and the power line are other future research topics. MLS has turned out to be a promising technique for the mapping of the trees in a forest environment [38], and could thus be used to map the vegetation in the power line corridors. Due to its viewing direction and data density and accuracy, MLS maps the forest around the power line corridor thoroughly and accurately—also below the forest canopy. Hence, the MLS data could be used to estimate prediction models for the vegetation growth, possibly complemented with the ALS and other remotely sensed data. The accurate vegetation growth models would provide valuable information for the planning of cost-effective maintenance operations for power line corridors.

Acknowledgment

The Academy of Finland supported this study through projects “Centre of Excellence in Laser Scanning Research” (decisions 307362, 292735), Multi-spectral personal laser scanning for automated environment characterization (decision 300066), “Integration of Large Multisource Point Cloud and Image Datasets for Adaptive Map Updating” (decision 295047), Multispectral mobile and UAV-based laser scanning (decision 307823), and through Strategic Research Council project “Competence-Based Growth Through Integrated Disruptive Technologies of 3D Digitalization, Robotics, Geospatial Information and Image Processing/Computing—Point Cloud Ecosystem” (decisions 293389 and 314312). We also acknowledge Business Finland for its support in project “VARPU” (7031/31/2016).

We thank Lic. tech. P. Litkey for the help with the Appendix A and Dr. X. Liang for the discussion about the study. We also thank the two anonymous reviewers for their valuable comments to improve the manuscript.

Appendix A. The number of the iterations inside Ransac

In this appendix, we derive a formula for the maximum number of iterations m in Ransac such that the probability of detecting a line is larger than some lower limit. The larger the value of m is, the higher is the probability that a line is detected. The aim is to first fix a desired lower limit p_{det} for the probability of detecting a line and then set the value of m such that this limit is exceeded. To do this, below we derive an expression for m as a function of p_{det}.

Let the task be to apply Ransac algorithm once to a point cloud (see details in Section 4.3) in order to find the smallest line, that is, the line that contains the least amount of points in the point cloud. Typically, the point cloud contains several power lines, but here we are interested to find only the smallest line. The reason for using the smallest line follows from the fact that we want to find the lower limit for the probability to find any line from a point cloud. The more a line contains points, the higher the probability is that the line is detected. Therefore, the probability of finding the smallest line is a lower limit for the probability of finding any line from the point cloud. Of course, the size of the smallest line is not known beforehand. However, we can estimate this size based on the minimum along-the-line point density (see Section 3.1) and minimum power line length.

Let us assume that the smallest line consists of k points $T = (t_1, \dots, t_k)$ and that a point cloud, which contains K points exists such that it contains the set T. If k and K are known, a probability p_{det} that the line is detected from the point cloud can be calculated as a function of m. Below, we first derive a formula for p_{det} as a function of m, k, and K. As this is the probability of detecting the smallest line, it is also the lower limit for finding any line from the point cloud. Second, we derive a formula for m as a function of p_{det}, k, and K, which is the objective of this appendix.

Let us assume that a point cloud exists, which contains K points in total and that the point cloud contains exactly one line, which consists of k points $T = (t_1, \dots, t_k)$. In one iteration of Ransac, two points u_1 and u_2 are randomly selected from the point cloud without replacement. An indicator variable A is defined such that

$$A \begin{cases} 1, & u_1, u_2 \in T \\ 0, & \text{either } u_1 \notin T \text{or } u_2 \notin T \text{or both} \end{cases}. \tag{A.1}$$

That is, the line of size k is detected if $A = 1$ and otherwise not. Let $p_1 = \mathrm{P}(A = 1)$, that is, the probability that A has a value of 1 and $p_0 = \mathrm{P}(A = 0)$. p_1 and p_0 can be expressed as a function of k and K using the equations

$$p_1 = \mathrm{P}(A = 1) = \frac{k}{K} \cdot \frac{(k-1)}{(K-1)} \tag{A.2}$$

$$p_0 = \mathrm{P}(A = 0) = 1 - p_1 \tag{A.3}$$

Let A_i be the value of A in iteration i of Ransac, $i = 1, \dots, m$. The probability of not detecting a line of size k in the first m iterations equals ${p_0}^m$. Hence, the probability of detecting the line in the first m iterations $p_{\text{det}} = 1 - {p_0}^m$. This equation can be solved for the variable m by using the identity $\log_a v = \ln v / \ln a$, where $a > 0$ is the base of the logarithm and $v > 0$:

$$p_{\text{det}} = 1 - {p_0}^m$$

$${p_0}^m = 1 - p_{\text{det}}$$

$$m = \log_{p_0}(1 - p_{\text{det}})$$

$$m = \frac{\ln(1 - p_{\text{det}})}{\ln p_0}$$

$$m = \frac{\ln(1 - p_{\text{det}})}{\ln(1 - p_1)}.$$

If we substitute p_1 into this equation from Eq. (A.2), we gain a formula for m as a function of p_{det}, k and K:

$$m = \left\{ \ln\left[1 - \frac{k(k-1)}{K(K-1)} \right] \right\}^{-1} \ln(1 - p_{\text{det}}). \tag{A.4}$$

If all the lines in the point cloud contain at least k points, the probability of detecting any of them will be p_{det} or higher if m iterations are performed in Ransac.

Appendix B. The pseudocode of the power line extraction algorithm

In this appendix, the algorithms for the power line extraction are presented as a pseudocode. The Algorithm B.1 is a parent function, which calls the other two functions, that is, Algorithm B.2 and Algorithm B.3. It is assumed that the indexing of an array starts from one, that is, $B(1)$ is the first element of the array B.

Algorithm B.1. Extract power line segments from a 3D point cloud.

Algorithm B.1 Extract power line segments from a 3D point cloud.
extractPowerLines(***pointCloud***, ***minLength***, ***minNumPtsCond***, n_{window}, ***maxNumRansacCalls***, ***maxNumIterRansac***, ***maxNormDistInlier***, ***maxGapLength***, ***maxAngleHor***, ***radiusLocalNeighCPL***)

Input: $pointCloud$: point cloud, which consists of n_{blocks} preprocessed blocks $pointCloud(i), i = 1, \ldots, n_{blocks}$; $minLength$: minimum length of a power line; $minNumPtsCond$: minimum number of points in a power line; n_{window}: search window size in the CPLS method; $maxNumRansacCalls$: the maximum number of consecutive calls of Ransac without finding a power line; $maxNumIterRansac$: the maximum number of the sampled line candidates in Ransac; $maxNormDistInlier$: the maximum normal distance for the inliers in Ransac; $maxGapLength$: maximum allowed gap in the connected component search; $maxAngleHor$: maximum angle of a power line with respect to the horizontal plane; $radiusLocalNeighCPL$: local neighborhood in CPLS.
Output: $PowerLines$: A list of found power line segments

```
1  for each block in pointCloud
2      Find power line candidate points from the block
3  end for
4  Initialize a list PowerLines for the found power lines
5  k ← 0 //initialize the index of the last found power line
6  for i ← 1 to n_blocks − 1 do
7      j ← 0 //counter for stopping the search
8      cand ← "power line candidates found from point
       cloud blocks i and i + 1"
9      while j < maxNumRansacCalls do
10         //Search for a line using Ransac
11         l ← Ransac2DLine(cand, maxNumIterRansac,
           maxNormDistInlier, minNumPtsCond)
12         if a line was found then
13             //Find longest connected power line segment
14             CPL ← CPLS(l, maxGapLength,
               maxAngleHor, n_window,
               radiusLocalNeighCPL)
15             if "length of CPL" ≥ minLength and "number
               of points in CPL" ≥ minNumPtsCond then
16                 k ← k + 1
17                 PowerLines(k) ← CPL
                   j ← 0
18                 Remove points in CPL from cand
19             else
20                 //no power line was found
21                 j ← j + 1
22             end if
23         else
24             //Ransac found no line; move to the next //block
25             j ← maxNumRansacCalls
26         end if
27     end while
28 end for
```

Algorithm B.2. CPLS algorithm, which finds a connected power line component from a Ransac line (see Section 4.3.1).

Algorithm B.2 CPLS algorithm, which finds a connected power line component from a Ransac line (see Section 4.3.1).
CPLS(l, $maxGapLength$, $maxAngleHor$, n_{window}, $radiusLocalNeighCPL$)

Input: l: line, which is output of Ransac2DLine (a set of 3D points); $maxGapLength$: maximum allowed gap in the connected component search; $maxAngleHor$: maximum angle with respect to the horizontal plane; n_{window}: search window in the CPLS method; ; $radiusLocalNeighCPL$: local neighborhood in CPLS.
Output: $CPL_{longest}$: the longest connected power line (CPL) (i.e., a connected line segment classified as a power line) found from the line l.

```
1  unlabeledPoints ← "Points in l"
2  Initialize list CPL_list //contains found CPLs
3  Order points in unlabeledPoints along the line l
4  while unlabeledPoints is not empty do
5      CPL ← "An initialized new empty CPL"
6      Initialize an empty array w for the n_window neighboring points after the last point
7      p_last ← "first point in unlabeledPoints" //Initialize the last point of the new CPL
8      w ← "n_window first points in unlabeledPoints"
9      for each point p in w do
10         if ("the horizontal distance between p and p_last" < maxGapLength and "the slope of the line joining p and p_last" < maxAngleHor) or ("the distance between p and p_last" < radiusLocalNeighCPL) then
11             Add p to CPL
12         end if
13     end for
14     while At least one new point from w was added to CPL do
15         p_last ← "last point of the CPL along the line l"
16         w ← "n_window consecutive points in unlabeledPoints starting from the next point after p_last",
17         for each point p in w do
18             if ("the horizontal distance between p and p_last" < maxGapLength and "the slope of the line joining p and p_last" < maxAngleHor) or ("the distance between p and p_last" < radiusLocalNeighCPL) then
19                 Add p to CPL
20             end if
21         end for
22     end while
23     Remove points in CPL from unlabeledPoints
24     Save CPL into list CPL_list
25 end while
26 CPL_longest ← "longest CPL in CPL_list"
```

Algorithm B.3. Find a 2D line using Ransac.

Algorithm B.3 Find a 2D line using Ransac.
Ransac2DLine($\boldsymbol{P}$, $\boldsymbol{maxNumIterRansac}$, $\boldsymbol{maxNormDistInlier}$, $\boldsymbol{minNumPtsLine}$)

Input: P: 2D point cloud; $maxNumIterRansac$: the maximum number of the sampled candidates; $maxNormDistInlier$: the maximum normal distance for the inliers; $minNumPtsLine$: the minimum number of points on a line

Output: l: line, that is, a set of points that lie on the line.

$n_{cand} \leftarrow 0$ //Initialize the number of sampled candidates
$lineFound \leftarrow$ **false**
while ($lineFound$ is **false**) **and** ($n_{cand} <$ $maxNumIterRansac$) **do**
  Select two points q_1 and q_2 from P randomly
  Calculate the normal distance of all points in P to the candidate line that travels through q_1 and q_2
  $inliers \leftarrow$ "Points whose normal distance to the line is less than $maxNormDistInlier$"
  if "the number of points in $inliers$" $>$ $minNumPtsLine$ **then**
    $lineFound \leftarrow$ **true**
    $l \leftarrow inliers$
  else
    $n_{cand} \leftarrow n_{cand} + 1$
  end if
end while

References

[1] R.K. Aggarwal, A.T. Johns, J.A.S.B. Jayasinghe, W. Su, An overview of the condition monitoring of overhead lines, Electric Power Systems Research [Online] 53 (1) (2000) 15–22, https://doi.org/10.1016/S0378-7796(99)00037-1.

[2] J. Ahmad, A.S. Malik, L. Xia, N. Ashikin, Vegetation encroachment monitoring for transmission lines right-of-ways: a survey, Electr. Power Syst. Res. 95 (2013) 339–352, https://doi.org/10.1016/j.epsr.2012.07.015.

[3] J. Ahmad, A.S. Malik, M.F. Abdullah, N. Kamel, L. Xia, A novel method for vegetation encroachment monitoring of transmission lines using a single 2D camera, Pattern Analysis and Applications [Online] 18 (2) (2014) 419–440, https://doi.org/10.1007/s10044-014-0391-9.

[4] E. Ahokas, H. Kaartinen, L. Matikainen, J. Hyyppä, H. Hyyppä, Accuracy of high-pulse-rate laser scanners for digital target models, Proceedings of the 21st European Association of Remote Sensing Laboratories (EARSeL) Symposium, Observing Our Environment from Space: New Solutions for a New Millennium, Balkema Publishers, Paris, France, 2002, pp. 175–178 https://www.maanmittauslaitos.fi/en/research/publications/publications-departments/remote-sensing-and-photogrammetry.

[5] M. Ax, S. Thamke, L. Kuhnert, K.-D. Kuhnert, UAV based laser measurement for vegetation control at high-voltage transmission lines, Adv. Mater. Res. 614–615 (2013) 1147–1152 [Online]. https://doi.org/10.4028/www.scientific.net/AMR.614-615.1147.

[6] P. Axelsson, Processing of laser scanner data—algorithms and applications, ISPRS J. Photogramm. Remote Sens. 54 (2–3) (1999) 138–147 [Online]. http://www.sciencedirect.com/science/article/pii/S0924271699000088?via%3Dihub https://doi.org/10.1016/S0924-2716(99)00008-8.

[7] J.-A. Beraldin, F. Blais, U. Lohr, Laser scanning technology, in: G. Vosselman, H.-G. Maas (Eds.), Airborne and Terrestrial Laser Scanning, Whittles Publishing, Dunbeath, Scotland, UK, 2010, pp. 1–42 (ISBN: 978-1-904445-87-6; 978-1-4398-2798-7; 1-904445-87-X). (Distributed in North America by CRC 2010).

[8] C.M. Bishop, Pattern Recognition and Machine Learning, Springer-Verlag, New York, NY, USA, 2006, pp. 563–565 (ISBN: 978-0-387-31073-2).

[9] R.C. Bolles, M.A. Fischler, "A Ransac-based approach to model fitting and its application to finding cylinders in range data," in Proceedings of the 7th International Joint Conference on Artificial Intelligence (IJCAI), Vancouver, Canada, 1981, pp. 637–643. http://dl.acm.org/citation.cfm?id=1623264.1623272; https://www.ijcai.org/Proceedings/81-2/Papers/009.pdf. Date of last access: 5.2.2019.

[10] C. Cabo, C. Ordoñez, S. García-Cortés, J. Martínez, An algorithm for automatic detection of pole-like street furniture objects from mobile laser scanner point clouds, ISPRS J. Photogramm. Remote Sens. 87 (2014) 47–56 [Online]. https://doi.org/10.1016/j.isprsjprs.2013.10.008.

[11] T. Chaperon, F. Goulette, Extracting cylinders in full 3D data using a random sampling method and the Gaussian image, Proceedings of the Vision Modeling and Visualization Conference, Stuttgart., Germany, 2001, pp. 35–42 http://citeseerx.ist.psu.edu/viewdoc/download?doi=10.1.1.23.5998&rep=rep1&type=pdf , Accessed date: 2 June 2019.

[12] L. Cheng, L. Tong, Y. Wang, M. Li, Extraction of urban power lines from vehicle-borne lidar data, Remote Sens. 6 (4) (2014) 3302–3320 [Online]. http://www.mdpi.com/2072-4292/6/4/3302 https://doi.org/10.3390/rs6043302.

[13] S. Clode, F. Rottensteiner, Classification of trees and powerlines from medium resolution airborne laserscanner data in urban environments, Proceedings of the APRS (The Australian Pattern Recognition Society) Workshop on Digital Image Computing (WDIC 2005), Brisbane, Australia, 2005, pp. 191–196 http://staff.itee.uq.edu.au/lovell/aprs/wdic2005/papers/17.pdf , Accessed date: 2 May 2019.

[14] R.O. Duda, P.E. Hart. (1972). Use of the Hough transformation to detect lines and curves in pictures. Communications of the ACM (Association for Computing Machinery). [Online]. 15(1), pp. 11–15. http://dl.acm.org/citation.cfm?id=361242; https://apps.dtic.mil/dtic/tr/fulltext/u2/a457992.pdf. Date of last access: 5.2.2019. https://doi.org/10.1145/361237.361242.

[15] M.A. Fischler, R.C. Bolles. (1981). Random sample consensus: a paradigm for model fitting with applications to image analysis and automated cartography. Communications of the ACM (Association for Computing Machinery). [Online]. 24(6), pp. 381–395. http://dl.acm.org/citation.cfm?id=358692; https://apps.dtic.mil/dtic/tr/fulltext/u2/a460585.pdf. Date of last access: 5.2.2019. https://doi.org/10.1145/358669.358692.

[16] C. Früh, S. Jain, A. Zakhor, Data processing algorithms for generating textured 3D building facade meshes from laser scans and camera images, International Journal of Computer Vision. [Online] 61 (2) (2005) 159–184 https://doi.org/10.1023/B:VISI.0000043756.03810.dd.

[17] H. Guan, Y. Yu, J. Li, Z. Ji, Q. Zhang, Extraction of power-transmission lines from vehicle-borne lidar data, Int. J. Remote Sens. 37 (1) (2016) 229–247 [Online]. http://www.tandfonline.com/doi/abs/10.1080/01431161.2015.1125549 https://doi.org/10.1080/01431161.2015.1125549.

[18] B. Guo, X. Huang, F. Zhang, G. Sohn, Classification of airborne laser scanning data using JointBoost, ISPRS Journal of Photogrammetry and Remote Sensing. [Online] 100 (2015) 71–83 (Refers to Publisher's Note ISPRS Journal of Photogrammetry and Remote Sensing, Volume 92, June 2014, Pages 124–136), https://doi.org/10.1016/j.isprsjprs.2014.04.015.

[19] N. Haala, M. Peter, J. Kremer, G. Hunter, Mobile lidar mapping for 3D point cloud collection in urban areas—A performance test, Proceedings of the XXIst ISPRS Congress, Beijing, China, The International Archives of the Photogrammetry, Remote Sensing and Spatial Information Sciences, 37(B5) 2008, pp. 1119–1124 http://www.riegl.co.at/uploads/tx_pxpriegldownloads/Streetmapper_ISPRS2008.pdf , Accessed date: 5 February 2019.

[20] Method, and means for recognizing complex patterns, by P.V.C. Hough. (1962, Dec 18). U.S. Patent 3069654. https://www.osti.gov/scitech/biblio/4746348. Date of last access: 5.2.2019.

[21] C.-W. Hsu, C.-C. Chang, C.-J. Lin, A practical guide to support vector classification, [Online]. http://www.csie.ntu.edu.tw/~cjlin/papers/guide/guide.pdf, (2016) , Accessed date: 5 February 2019.

[22] J. Hyyppä, A. Jaakkola, Y. Chen, A. Kukko, H. Kaartinen, L. Zhu, P. Alho, H. Hyyppä, Unconventional LIDAR mapping from air, terrestrial and mobile, Proceedings of the Photogrammetric Week, Stuttgart., Germany, 2013, pp. 205–214 http://www.ifp.uni-stuttgart.de/publications/phowo13/180hyyppae.pdf , Accessed date: 5 February 2019.

[23] H. Hyötyniemi, Multivariate Regression—Techniques and Tools, 125 Helsinki University of Technology, Control Engineering Laboratory, Helsinki, Finland, 2001 Report. Available: http://neocybernetics.com/report125/ , Accessed date: 2 May

2019.
[24] A. Jaakkola, J. Hyyppä, A. Kukko, X. Yu, H. Kaartinen, M. Lehtomäki, Y. Lin, A low-cost multi-sensoral mobile mapping system and its feasibility for tree measurements, ISPRS J. Photogramm. Remote Sens. 65 (6) (2010) 514–522 [Online]. https://doi.org/10.1016/j.isprsjprs.2010.08.002.
[25] A. Jaakkola, J. Hyyppä, X. Yu, A. Kukko, H. Kaartinen, X. Liang, H. Hyyppä, Y. Wang, Autonomous collection of Forest field reference—the outlook and a first step with UAV laser scanning, Remote Sens. 9 (8) (2017), https://doi.org/10.3390/rs9080785 [Online]. Available: http://www.mdpi.com/2072-4292/9/8/785/htm.
[26] Y. Jwa, G. Sohn, A piecewise catenary curve model growing for 3D power line reconstruction, Photogramm. Eng. Remote. Sens. 78 (12) (2012) 1227–1240 [Online]. 10.14358/PERS.78.11.1227.
[27] H. Kaartinen, J. Hyyppä, A. Kukko, A. Jaakkola, H. Hyyppä, Benchmarking the performance of mobile laser scanning systems using a permanent test field, Sensors 12 (9) (2012) 12814–12835 [Online]. https://doi.org/10.3390/s120912814.
[28] H. Kaartinen, J. Hyyppä, M. Vastaranta, A. Kukko, A. Jaakkola, X. Yu, J. Pyörälä, X. Liang, J. Liu, Y. Wang, R. Kaijaluoto, T. Melkas, M. Holopainen, H. Hyyppä, Accuracy of kinematic positioning using global satellite navigation systems under forest canopies, Forests 6 (9) (2015) 3218–3236 [Online]. https://doi.org/10.3390/f6093218.
[29] E. Kim, G. Medioni, Urban scene understanding from aerial and ground LIDAR data, Mach. Vis. Appl. 22 (4) (2011) 691–703 [Online]. https://doi.org/10.1007/s00138-010-0279-7.
[30] H.B. Kim, G. Sohn, Point-based classification of power line corridor scene using random forests, Photogrammetric Engineering & Remote Sensing. [Online] 79 (9) (2013) 821–833 10.14358/PERS.79.9.821.
[31] I. Klein, S. Filin, "LiDAR and INS fusion in periods of GPS outages for mobile laser scanning mapping systems," in Proceedings of the ISPRS Workshop Laser Scanning 2011, Calgary, Canada, 2011, pp. 231–236. The International Archives of the Photogrammetry, Remote Sensing and Spatial Information Sciences, 38(5)/W12. Available: https://pdfs.semanticscholar.org/f020/2d422c2978ff20323d4bf7fc3b8ce728afa4.pdf. Date of last access: 5.2.2019. doi:https://doi.org/10.5194/isprsarchives-XXXVIII-5-W12-231-2011.
[32] Y. Kobayashi, G. Karady, G. Heydt, R. Olsen, The utilization of satellite images to identify trees endangering transmission lines, IEEE Transactions on Power Delivery 24 (3) (2009) 1703–1709 [Online]. https://doi.org/10.1109/TPWRD.2009.2022664.
[33] A. Kukko, C.-O. Andrei, V.-M. Salminen, H. Kaartinen, Y. Chen, P. Rönnholm, H. Hyyppä, J. Hyyppä, R. Chen, H. Haggrén, I. Kosonen, K. Čapek, Road environment mapping system of the Finnish geodetic institute—FGI roamer, Proceedings of the ISPRS Workshop 'Laser Scanning 2007 and SilviLaser 2007', Espoo, Finland, The International Archives of the Photogrammetry, Remote Sensing and Spatial Information Sciences, XXXVI–3/W52, 2007, pp. 241–247 http://www.isprs.org/proceedings/XXXVI/3-W52/final_papers/Kukko_2007b.pdf , Accessed date: 5 February 2019.
[34] A. Kukko, H. Kaartinen, J. Hyyppä, M. Zanetti, Backpack personal laser scanning system for grain-scale topographic mapping, Proceedings of the 46th Lunar and Planetary Science Conference, March 16–20 2015, the Woodlands, Texas, USA, Abstract #2407, 2015 https://www.hou.usra.edu/meetings/lpsc2015/eposter/2407.pdf also in https://www.hou.usra.edu/meetings/lpsc2015/pdf/2407.pdf , Accessed date: 5 February 2019Permalink: http://hdl.handle.net/10138/224728.
[35] A. Kukko, R. Kaijaluoto, H. Kaartinen, V.V. Lehtola, A. Jaakkola, J. Hyyppä, Graph SLAM correction for single scanner MLS forest data under boreal forest canopy, ISPRS J. Photogramm. Remote Sens. 132 (2017) 199–209 [Online]. https://doi.org/10.1016/j.isprsjprs.2017.09.006.
[36] M. Lehtomäki, A. Jaakkola, J. Hyyppä, A. Kukko, H. Kaartinen, Detection of vertical pole-like objects in a road environment using vehicle-based laser scanning data, Remote Sensing. [Online] 2 (3) (2010) 641–664 https://doi.org/10.3390/rs2030641.
[37] M. Lehtomäki, A. Jaakkola, J. Hyyppä, J. Lampinen, H. Kaartinen, A. Kukko, E. Puttonen, H. Hyyppä, Object classification and recognition from mobile laser scanning point clouds in a road environment, IEEE Trans. Geosci. Remote Sens. 54 (2) (2016) 1226–1239 [Online]. https://doi.org/10.1109/TGRS.2015.2476502.
[38] X. Liang, J. Hyyppä, A. Kukko, H. Kaartinen, A. Jaakkola, X. Yu, The use of a mobile laser scanning system for mapping large forest plots, IEEE Geosci. Remote Sens. Lett. 11 (9) (2014) 1504–1508 [Online]. https://doi.org/10.1109/LGRS.2013.2297418.
[39] Y. Lin, J. Hyyppä, T. Rosnell, A. Jaakkola, E. Honkavaara, Development of a UAV-MMS-collaborative aerial-to-ground remote sensing system – a preparatory field validation, IEEE Journal of Selected Topics in Applied Earth Observations and Remote Sensing. 6 (4) (2013) 1893–1898 [Online]. https://doi.org/10.1109/JSTARS.2012.2228168.
[40] L. Matikainen, M. Lehtomäki, E. Ahokas, J. Hyyppä, M. Karjalainen, A. Jaakkola, A. Kukko, T. Heinonen, Remote sensing methods for power line corridor surveys, ISPRS J. Photogramm. Remote Sens. 119 (2016) 10–31 [Online]. https://doi.org/10.1016/j.isprsjprs.2016.04.011.
[41] R.A. McLaughlin, Extracting transmission lines from airborne LIDAR data, IEEE Geosci. Remote Sens. Lett. 3 (2) (2006) 222–226 [Online]. https://doi.org/10.1109/LGRS.2005.863390.
[42] T. Melzer, C. Briese, Extraction and modeling of power lines from ALS point clouds, Proceedings of the 28th Workshop of the Austrian Association for Pattern Recognition, Hagenberg., Austria, 2004, pp. 47–54 https://publik.tuwien.ac.at/files/PubDat_119606.pdf , Accessed date: 6 February 2019.
[43] S.J. Mills, M.P.G. Castro, Z. Li, J. Cai, R. Hayward, L. Mejias, R.A. Walker, Evaluation of aerial remote sensing techniques for vegetation management in power-line corridors, IEEE Trans. Geosci. Remote Sens. 48 (9) (2010) 3379–3390 [Online]. https://doi.org/10.1109/TGRS.2010.2046905.
[44] V.S. Murthy, S. Gupta, D.K. Mohanta, Digital image processing approach using combined wavelet hidden markov model for well-being analysis of insulators, IET Image Processing [Online] 5 (2) (2011) 171–183 https://doi.org/10.1049/iet-ipr.2009.0293.
[45] G. Petrie, An introduction to the technology: mobile mapping systems, Geoinformatics 13 (1) (2010) 32–43 https://search.proquest.com/openview/b6b8c2a2ef8cf9a354184357512977fb/1?pq-origsite=gscholar&cbl=178200 , Accessed date: 5 February 2019.
[46] I. Puente, H. González-Jorge, J. Martínez-Sánchez, P. Arias, Review of mobile mapping and surveying technologies, Measurement [Online] 46 (7) (2013) 2127–2145 https://doi.org/10.1016/j.measurement.2013.03.006.
[47] S.S. Rao, Optimization: Theory and Applications, 2nd ed, Wiley Eastern Limited, New Delhi, India, 1984, pp. 223–224 (ISBN: 0-85226-780-0).
[48] J.P. Royston, An extension of Shapiro and Wilk's *W* test for normality to large samples, Appl. Stat. 31 (2) (1982) 115–124 [Online]. https://doi.org/10.2307/2347973.
[49] J.P. Royston, Algorithm AS 177: expected normal order statistics (exact and approximate), Appl. Stat. 31 (2) (1982) 161–165 [Online]. https://doi.org/10.2307/2347982.
[50] M. Rutzinger, A.K. Pratihast, S. Oude Elberink, G. Vosselman, Tree modelling from mobile laser scanning data-sets, Photogrammetric Record. [Online] 26 (135) (2011) 361–372 https://doi.org/10.1111/j.1477-9730.2011.00635.x.
[51] R. Schnabel, R. Wahl, R. Klein, Efficient Ransac for point-cloud shape detection, Computer Graphics Forum 26 (2) (2007) 214–226 [Online]. https://doi.org/10.1111/j.1467-8659.2007.01016.x.
[52] A. Shafieezadeh, U.P. Onyewuchi, M.M. Begovic, R. DesRoches, Age-dependent fragility models of utility wood poles in power distribution networks against extreme wind hazards, IEEE Transactions on Power Delivery. [Online] 29 (1) (2014) 131–139 https://doi.org/10.1109/TPWRD.2013.2281265.
[53] S.S. Shapiro, M.B. Wilk, An analysis of variance test for normality (complete samples), Biometrika [Online] 52 (3/4) (1965) 591–611 https://doi.org/10.2307/2333709.
[54] Z. Tang, C. Zhou, W. Jiang, W. Zhou, X. Jing, J. Yu, B. Alkali, B. Sheng, Analysis of significant factors on cable failure using the cox proportional hazard model, IEEE Transactions on Power Delivery. [Online] 29 (2) (2014) 951–957 https://doi.org/10.1109/TPWRD.2013.2287025.
[55] H.C. Thode Jr., Testing for Normality. New York, NY, USA: Marcel Dekker, 2002, pp. 27–29. (ISBN: 0-8247-9613-6).
[56] M. Yadav, C.G. Chousalkar, Extraction of power lines using mobile LiDAR data of roadway environment, Remote Sensing Applications: Society and Environment [Online] 8 (2017) 258–265 https://doi.org/10.1016/j.rsase.2017.10.007.
[57] L. Zhu, J. Hyyppä, Fully-automated power line extraction from airborne laser scanning point clouds in forest areas, Remote Sensing [Online] 6 (11) (2014) 11267–11282 https://doi.org/10.3390/rs61111267.